INVESTIGATIONS OF RADIATION-INDUCED AND CARRIER-ENHANCED CONDUCTIVITY*

A. Meulenberg, Jr.
COMSAT Laboratories
Clarksburg, Maryland 20734

L. W. Parker
Lee W. Parker Inc.
Concord, Massachusetts 01742

E. J. Yadlowski and R. C. Hazelton
H-Y Tek Corporation
Radford, Virginia 24143

A steady-state carrier computer code, PECK (Parker-Enhanced Carrier Kinetics), that predicts the radiation-induced conductivity (RIC) produced in a dielectric by an electron beam was developed. The model, which assumes instantly-trapped holes, was then applied to experimental measurements on thin Kapton samples penetrated by an electron beam. Measurements at high bias were matched in the model by an appropriate choice for the trap-modulated electron mobility ($\mu' \simeq 7 \times 10^{-15}$ m^2/V-s). A fractional split between front and rear currents measured at zero bias is explained on the basis of beam-scattering.

The effects of carrier-enhanced conductivity (CEC) on data obtained for thick, free-surface Kapton samples is described by using an analytical model that incorporates field injection of carriers from the RIC region. The computer code, LWPCHARGE, modified for carrier transport, is also used to predict partial penetration effects associated with CEC in the unirradiated region. Experimental currents and surface voltages, when incorporated in the appropriate models, provide a value for the trap-modulated mobility ($\mu' = 3-7 \times 10^{-15}$ m^2/V-s) that is in essential agreement with the RIC results.

I. INTRODUCTION

The theoretical studies reported here were undertaken to establish carrier models for the proper interpretation of experimental data. These studies provide conductivity formulae for thin (ref. 1) and thick Kapton (ref. 1,2) samples in electron beams. ("Thin" here refers to sample thickness smaller than or comparable to the electron range; "thick" refers to sample thickness larger than the electron range.)

The thin-Kapton experiments were designed to evaluate the RIC by subjecting a biased sample with metallized surfaces to a penetrating electron beam and measuring the currents from the front surface (beam side) and rear surface (substrate side). In the thick-Kapton experiments, the front surface was not metallized but was free to float at a surface potential determined by the balance of incident, backscatter,

---

*This paper is based on work performed under the sponsorship and technical direction of the International Telecommunications Satellite Organization (INTELSAT). Views expressed are not necessarily those of INTELSAT.

secondary, and conduction currents. The thick-Kapton experiments were designed to measure secondary yields from the "free" surface and enhanced bulk conductivity, the latter characterizing the nonpenetrated region (comprising most of the sample thickness). The enhancement results from the presence of additional carriers supplied from the irradiated region. The modeling of the CEC and of the RIC is the goal of the present study.

II. RADIATION-INDUCED CONDUCTIVITY

Electron-hole pairs produced by energetic electrons penetrating a dielectric sample sandwiched between metal plates can recombine or separate to become negative and positive free carriers.* These carriers undergo one of three ultimate fates:

a. While free, they can exit the sample by "drifting" under the influence of an electric field (applied plus space charge) or by "diffusing" (random walk) to one of the plates.

b. They can "fall into" (be captured by) a deep trap (localized state) with energy, well below the free electron level. This process effectively immobilizes them, but their presence contributes to the space charge.

c. They can vanish by recombining with an already captured immobile carrier of the opposite sign, also eliminating the trapped carrier.

Fate (b) can be modified by the thermal release ("detrapping") of the trapped carrier. The probability of detrapping depends on temperature, electric field, and trap energy. A free carrier can undergo a series of trapping and detrapping events (more probable with shallow traps than with deep traps) until it is eliminated by fate (a) or fate (b) above. Fate (c) can also include recombination with a free carrier of the opposite sign, but this option is much less probable than recombination with the much more numerous trapped carriers. The notation used in this study is defined as follows:

p, n = concentrations of free holes and free electrons
p_T, n_T = concentrations of trapped holes and electrons
D_p, D_n = diffusion coefficients for free holes and electrons
M, μ = mobilities for free holes and electrons
R_1, R_2 = recombination coefficients (cm^3/s) for free holes with trapped electrons and free electrons with trapped holes
P_T, N_T = concentrations of neutral hole traps and neutral electron traps
E = electric field intensity
V = electric potential
e = magnitude of electron or hole charge
G = production rate of electron-hole pairs (per unit volume) associated with ionization dose rate (G')
H = deposition rate of injected carriers (excess charge assumed here to be electrons only)
ε = dielectric permittivity

---

*The terms "hole" or "positive free carrier" used here do not necessarily convey the same meaning as in semiconductor theory. They denote temporally stable positive charge sites; in some dielectrics, this uncompensated positive charge is more likely than a negative charge site to migrate.

τ_p, τ_n = mean lifetimes of free holes and electrons in the conduction band (i.e., time interval between introduction and trapping or "trapping times")

τ_+, τ_- = mean lifetimes of trapped holes and electrons (i.e., time between trapping and release or "detrapping times")

F_p, F_n = fluxes of holes and electrons

J_p, J_n = current densities of holes and electrons ($J = eF$).

The transport and Poisson equations are set up in standard fashion (ref. 3-6) with appropriate boundary conditions and approximations made to help solve the system of differential equations. The complete formulation is given in reference 7.

In our preliminary work on Kapton, we made the following simplifications to more easily understand the carrier kinetics. One simplification is the use of a steady-state solution. We also assume that the holes are instantly trapped (and not released) and that the electrons are not deeply trapped (at most, shallowly trapped and detrapped). Thus, the electrons may be considered quasi-free, but the trapping/detrapping effects inhibit their motion, which is described by replacing the true mobility μ by a much smaller "trap-modulated" effective mobility μ'. This leads to the following system of equations (ref. 7):

$$p = n_T = 0 \text{ (no holes or deeply trapped electrons)} \tag{1}$$

$$\frac{\partial f_p}{\partial x} = 0 \text{ (no hole migration)} \tag{2}$$

$$p_T = \frac{G}{nR_2} \text{ (trapped hole profile)} \tag{3}$$

$$\frac{\partial f_n}{\partial x} = H \text{ (electron flux gradient)} \tag{4}$$

$$\frac{d^2V}{dx^2} = -\frac{e}{\varepsilon}(n - p_T) \tag{5}$$

We define $E = -dV/dx$ and arrive at the expression

$$\frac{\mu kT}{e}\frac{d^2n}{dx^2} - \mu E \frac{dn}{dx} + H + \frac{\mu e}{\varepsilon}\left(\frac{G}{R_2} - n^2\right) = 0 \tag{6}$$

The first term is associated with electron diffusion, the second with electron drift, the third with electron deposition, and the fourth with space charge. These equations may be solved by numerical integration, subject to boundary conditions:

$n = 0$ at $x = 0$ and L (diffusion boundary condition)

$V = 0$ at $x = L$ (grounded substrate)

$V = V_A$ at $x = 0$ (applied bias voltage)

573

If injection occurs, one of the latter two conditions above is replaced by a prescribed value of dV/dx at the injection contact.

The method of solving differential equations (5) and (6) used here employs an iterative process. Enforcement of the above boundary conditions is accomplished by starting at x = 0 with initial values n = 0 and V = V_A, and with estimated values of dn/dx and dV/dx. The differential equations are then stepped to x = L with the intention of hitting n = 0 and V = 0 there as the "target" values. If these targets are not hit, we start again at x = 0 with readjusted values for dn/dx and dV/dx. If injection occurs, the initial or target conditions are suitably modified. This procedure is implemented in the computer code PECK. Under most conditions, the task of achieving the "converged" solution is not trivial, since there are two free starting variables. The solutions obtained, however, provide insight into the excess charge and electric fields in an irradiated dielectric.

III.   APPLICATION OF THE RIC MODEL TO THE THIN-KAPTON EXPERIMENT

This section presents an implementation of the trapped-hole RIC model, sample solutions, and a comparison of the model with experimental results.

The collected currents in the RIC experiment described below (and in ref. 1) were not symmetric with respect to applied bias. Therefore, the conductivity inferred from these data was found to be polarity dependent. Moreover, at zero bias, the rear current was observed to be larger than the front current. (This possibility had been predicted theoretically for sufficiently high-beam energies by Oliveira and Gross (ref. 8), and was seen in experiments on mica by Spear (ref. 9). Oliveira and Gross predicted total current collection at the rear contact when the beam voltage exceeded 35 keV. Aris et al. (ref. 10) considered the Oliveira and Gross theory as well as the Spear experiments, but they did not address the question of why they differ on the rear-front current split. The question is resolved in this study: the current split is associated with the degree of beam-scattering in the sample. The polarity dependence found in the RIC experiment is also explained here, by considering carrier injection, internal fields, and spatially varying conductivities.

A.   Experimental Data for Thin Kapton Samples (6.4 µm)

Figures 1 and 2 show variations in the front and rear current densities, J_1 and J_2, with varying net incident beam currents for fixed biases (±196 V and ±45 V) applied to the front surface. Here, J_B' denotes the beam current density, less the backscatter and secondary emission from the front surface. This can also be considered the net beam current entering the sample. The beam energy is 28 keV. Electrons moving toward the right are considered positive current. The superscript denotes the sign of the bias that has been applied to the front contact (number 1). Since J_1 and J_2 can exceed J_B', a source of electrons other than the beam must be invoked.

B.   Primary Current and Deposition Curves from
Theoretical Transport Model

By the use of a Monte Carlo transport code, tabulations were made of the particle and energy fluxes, which were then fitted as analytic functions of depth and net incident energy (ref. 1). The curve shown in figure 3 is the percentage of incident flux F vs depth x. This percentage is normalized to represent the fraction of a

1 nA/cm^2 28-keV incident beam that has penetrated to depth x in the sample. At the surface (x = 0), the value is 0.934, the fraction 0.066 having been lost to back-scatter. (The secondary emission has been ignored here since it is negligible for a high-energy beam.) The primary flux falls off monotonically to 0.023 at 6.4 μm.

Figure 4 shows the dose rate (G') in rads vs depth, obtained from the derivative of the energy flux as a function of x (not shown), and the excess-charge deposition rate (H) obtained from the derivative of the primary flux shown in figure 3. These two functions are similar to those plotted by Matsuoka et al. (ref. 11) in normalized form. The average and peak values of G' are 2,900 and 3,700 rad/s, respectively. The average and peak values of H are 0.14 and 0.21 nA/μm, respectively. (Here, G' denotes dose rate, while G denotes pair production or generation rate.)

C. Parameters of the Model

In the preliminary solutions of equations (5) and (6) that follow, for simplicity, constant values of G' and H, 2,900 rad/s and 0.16 nA/μm, respectively, have been assumed. The assumed constant deposition function H corresponds to a penetrating flux that decreases linearly with depth (extreme scattering), which helps in making analytical approximations. The following parameters were also used to model the experiment in the PECK code:

$$L = \text{thickness} = 6.4 \times 10^{-6} \text{ m} = 6.4 \text{ μm}$$
$$kT/e \text{ at room temperature} = 25 \text{ mV}$$
$$J_B = \text{nominal beam current} = 10^{-5} \text{ A/m}^2 = 1 \text{ nA/cm}^2$$
$$(F_B = \text{flux} = 6.25 \times 10^{13} \text{ electrons/m}^2\text{-s})$$
$$\varepsilon = \text{permittivity} = 3.4\varepsilon_0 = 3.4 \times 0.884 \times 10^{-11}$$
$$= 3.0 \times 10^{-11} \text{ F/m}$$
$$G = \text{pair generation rate} = 3 \times 10^{21}/\text{m}^3\text{-s}$$
$$= 3 \times 10^{15}/\text{cm}^3\text{-s}$$
$$R_2 = \text{recombination coefficient for free electrons}$$
$$\text{with trapped holes} = 10^{-13} \text{ m}^3/\text{s} = 10^{-7} \text{ cm}^3/\text{s}$$
$$\mu = \text{mobility} = \text{variable (in m}^2/\text{V-s)}.$$

The generation rate is based on our own transport calculations and on values found in the literature. For a 28-keV beam of current density, 1 nA/cm^2, a mean dose rate of 2,900 rad/s in the 6.4-μm Kapton sample was calculated. For a density of 1.43 g/cm^3, this dose rate translates to 2.6×10^{17} eV/cm^3-s. Now, choosing the energy per hole-electron pair (ref. 12) to be 100 eV yields G = 2.6×10^{15} pairs/cm^3-s. Rounding this to 3×10^{15} pairs/cm^3-s yields the value also used by Hughes for a SiO$_2$ photoconduction problem (ref. 4,5). The recombination coefficient is taken to be $R_2 = 10^{-7}$ cm^3/s; hence, $G/R_2 = 3.0 \times 10^{22}/\text{cm}^6 = 3.0 \times 10^{34}/\text{m}^6$.

IV. PRELIMINARY SOLUTIONS FROM THE TRAPPED-HOLE RIC MODEL

A. Zero Bias and Excess Charge Deposition

To gain experience and test the results, the computer model was tested for the simplest cases first. The first set of conditions included the use of constant G and H, no carrier injection from the contacts, and zero bias. Figure 5 illustrates the results under these conditions. The average excess electron concentration, n, exceeds the trapped hole concentration, and a negative potential, V, results inside the dielectric. The symmetry seen in fig. 5 is to be expected with the above conditions.

A series of runs was carried out, varying the value of mobility, μ. For $\mu > 0.88 \times 10^{-8}$ m^2/V-s, the excess electron population drains until a positive potential within the dielectric establishes equilibrium with the incident electron beam. For $\mu < 0.88 \times 10^{-8}$ m^2/V-s, a negative internal potential (fig. 5) develops to push out enough electrons to establish equilibrium with the beam-deposited electrons. As will be seen later, values of μ are much less than 10^{-8} m^2/V-s, so that a significant negative potential is expected within the bulk of a dielectric in an electron beam. This negative internal potential would prevent injection of electrons from the contacts into the dielectric. Our assumption of immobile holes prevents hole injection.

The electron fluxes, F for the primary flux from the beam, F_{DD} for the diffusion + drift flux, and F_{TOT} (= F + F_{DD}) provide a 50-50 split in the front and back contact currents $|J_1| = |J_2|$. No change in beam current density J_B or in carrier mobility will alter this balance. However, a change in the shape of G and/or H will affect it. If H shifts, depositing more charge in the rear of the film, the back current, J_2, will increase. If G shifts so that deposited energy, ionization, and conductivity is increased in the front half of the film, the front current, J_1, will increase. Both shifts are necessary to bring the model into closer agreement with the experimental conditions (depicted in fig. 4). Since the results of these shifts are in opposition, the relative importance of G and H are indicated by the experimental data showing $|J_2| > |J_1|$. If a nonlinear (cubic) form for H is used to better approximate the actual value from the 28-keV beam, the resultant distributions (charge, potential, and so on) will be similar in shape and magnitude to the linear case. However, an asymmetry sufficient to cause a 66/34-percent split between the back/front contact currents occurs. (The no-scattering approximation, which assumes no charge deposition except at the end of range, provides for total current collection at the back contact with sufficiently high-beam energies, as described in ref. 8.)

In the zero-bias case, the internal potential established by H is more important than the conductivity created by G, but as bias is applied, the situation changes. The field of an applied bias can exceed that generated by the trapped charge resulting from H. As the externally applied field gets larger, the conductivity provided by G has the greatest effect on the internal potential profiles and, therefore, on the current distribution.

The net current out of a film ($|J_1| + |J_2|$) must equal the total current into the film (J_B') if no bias is applied. The shapes of G and H will alter the relative currents to the two contacts (J_1 and J_2). Only if a bias is applied and injection of carriers from one or both contacts occurs can either J_1 or J_2 exceed J_B'.

B. 200-V Bias and Excess Charge Deposition

Experimental results of the penetrating electron beam on a thin Kapton film with a bias voltage (±196 V) applied (fig. 1) showed that all currents exceeded the beam current J_B, and therefore that injection of one form or another must be invoked. A computer fit was made to the experimental data with our simplified model (H and G constant), with high carrier injection from the contacts assumed, and with a +200 V bias applied to the front surface. The beam current deposited into the film was J_B' = 1 nA/cm^2; from Figure 1, J_1 and J_2 are -4.4 and 3.4 nA/cm^2, respectively.

The results of the fit are shown in figure 6. The high electron concentration adjacent to the negative contact extends into the bulk of the film and dominates the

beam-deposited charge through much of the dielectric. The effective mobility necessary to fit the model results to experimental results was $\mu' \approx 7 \times 10^{-15}$ m^2/V-s. This value must be considered crude because the model did not match the experimental conditions well; some constants [R_2 and G from eq. (5)] are values for SiO_2; and the injection represented is an extreme. Despite simplification of the model, some useful predictions can be made. The curvature of the potential within the film reflects the shape seen in figure 5 for the zero-bias case. At some positive bias, the slope of this curve is zero (dV/dx = 0) at the back contact; at some negative bias, dV/dx = 0 at the front contact. As the bias is varied through these critical points, the potential gradient reverses as does the current at that contact. The symmetry of the simplifying assumptions predicts a symmetry in the forward and reverse bias results of the model. However, the experimental results indicate more current flows when negative bias is applied to the front surface than when a positive bias is applied. The shape of G and H must therefore be important. The deposited charge and ionization-induced conductivity are significant relative to the bias-injected charge under the test conditions. If this is the case, when the bias voltage is reduced, the effects of G and H, relative to the effects of bias magnitude and polarity, should increase.

C. ±45-V Bias and Excess Charge Deposition

Experimental data are available for the lower bias situation (fig. 2). When compared with figure 1, it is seen that at the higher beam currents, one of the contact currents (J_2^+) reverses and crosses the J = 0 axis, as predicted by the model (see above). At even lower bias voltages, J_1^- would also be expected to cross over the J = 0 axis. This crossover results from a deposited charge that establishes fields which oppose and exceed the field created by the applied bias. Since values of conductivity are experimentally determined from the measured currents and applied voltages, care must be taken in dielectrics where internal fields can be reversed (and maintained) by the presence of excess (or trapped) charge. Assumptions about uniform fields and conductivities in electron-beam irradiated dielectrics are only valid under special conditions (e.g., if the beam intensity is low enough, the deposited charge will not greatly alter the potential profile compared to the effect of the bias). In figure 2, the beam current density of 0.65 nA/cm^2 is adequate to create a field at the back contact equal to that created by the +45-V bias on the 6.4-µm sample (hence, no current flows in this region). If no current is detected (J_2 = 0) and if uniform fields are assumed, it could appear that the conductivity is zero. This is obviously not the case. Similarly, under different conditions, interpretation of other effects (such as field and dose dependence) can be incorrect.

This study concludes that measurements of RIC, field-enhanced conductivity, and dose-dependent effects are unreliable in electron beam experiments without a proper model that reveals the internal potential profiles. Even irradiation with gamma-rays is a problem because of the effects of knock-on and back-scattered electrons (ref. 13).

D. Discussion of RIC Results

Several important facts emerged from the interpretation and modeling of the RIC experiment. First, injection of carriers from the contacts must be considered, at least in Kapton with gold contacts (some materials and some contacts might not permit injection). Second, with so many unknowns in the model, to determine material parameters, it is necessary to have as many experiments that vary the independent variables as there are unknowns to be found. Simplified computer models are very useful

in predicting the types of effects; however, more realistic values for G and H must be inserted to obtain realistic and quantitative values for the material parameters sought.

A brief recapitulation of the important factors in the model and experiment follows.

a. Assumptions about mobile negative charge and deeply trapped positive charge seem to fit the data for Kapton.

b. Depositing negative charge (with low mobility after deposition) means that a negative potential is created in the bulk of the dielectric.

c. With applied bias, injection of negative charge from the negative contact into the dielectric is required to fit the data.

d. The potential profiles in a film depend on the amount of charge deposited from the beam, injection from the contacts, local conductivity, and external bias (fig. 4-6); they are seldom linear.

e. Because of nonlinearities in charge deposition (H), carrier generation from energy deposition (G, which affects conductivity), and internal potentials, $V(x)$, external currents may be dominated by small regions of the dielectric. Material parameters cannot be accurately determined without accounting for these effects.

Two additional factors help explain the experimental data; these are described here more fully.

f. Contact currents J_1 and J_2 can be broken into components $J_{1,2}^V$ and $J_{1,2}^i$, which are composed of charge from the beam and charge injected from one contact or the other. Figure 7 contains two sets of current density components (beam generated and bias generated) for the simplified model. In cases of no applied bias, the beam-generated contact currents $|J_{1,2}^0|$ are equal, since G and H are uniform. In addition, $|J_1^0| + |J_2^0| = J_B$, and no injected component is present. With applied bias V, the beam-generated currents shift so that $|J_1^V| \neq |J_2^V|$; but they still add up to J_B. Injection currents ($J_{1,2}^i$ are the dotted line) flow from the negative contact and $J_1^i = J_2^i$. (The convention used here is that positive currents are described by electrons moving to the right in figure 1, therefore, injected currents have the same sign and the beam-generated currents have opposite signs.) The total contact currents are the sums of the components: $J_1^- = J_1^i + J_1^{V-}$; $J_2^- = J_2^i + J_2^{V-}$. Figure 7 shows the results of no bias applied and negative bias applied to the front (number 1) contact. Because of the assumptions, the same positive bias applied to the front contact would result in $J_1^+ = -J_2^-$ and $J_2^+ = -J_1^-$.

Figure 8 shows the component currents for a smaller positive bias. The negative values of the current sums $-J_1^+ = -(J_1^i + J_1^+)$ and $-J_2^+ = -(J_2^i + J_2^+)$ are displayed to make comparison with figures 1 and 2 easier. The reason for the $-J_2^+$ crossover may be easily seen from the summation of its components. Again, reversing the bias polarity provides $J_1^- = J_2^+$ and $J_2^- = J_1^+$ for this simplified model.

The condition $|J_1^V| + |J_2^V| = J_B'$ requires that $|J_{1,2}^V| \leq J_B'$. Figure 7 illustrates the basis for defining bias-dominated and beam-dominated regions. At a given bias, low-beam currents do not significantly alter the applied fields. However, with high-

beam currents, the deposited charge generates fields greater than those from the applied bias, at which point, charges also flow toward the negative contact and the dielectric becomes beam dominated (fig. 8).

The total current density curves in figures 7 and 8 are symmetric with positive and negative applied bias. Experimental results in figures 1 and 2, however, do not display this symmetry. The asymmetry seen in those figures is a result of nonuniform ionization and charge deposition profiles (G and H in fig. 4). Part of the effect results from the higher back contact current ($|J_2^0| > |J_1^0|$ at zero bias), which will make $|J_2^-| > |J_1^+|$ and $|J_1^-| > |J_2^+|$. However, differences observed in the experimental data are too great to be explained by this effect alone. An important additional effect involves the field injection of charge into the region of lower ionization near the back contact. To account for the experimental results, more electrons must flow from the irradiated bulk (under negative front bias) than from the metallic contact (under positive front bias). The data base is not adequate to determine if the difference is dominated by different field strengths in the injection region (with bias reversal) or by different charge-release mechanisms (irradiated dielectric vs metal contact).

g. The apparent saturation of injection current (fig. 7 and 8) is attributed primarily to a change from an n to an $n^{1/2}$ dependence of conductivity with an increasing beam current (ref. 12).

With increasing carrier generation, the principal loss mechanism of electrons changes from shallow traps to recombination with trapped holes (ref. 12). Other effects, which make an actual determination of conductivity dependence-on-dose very difficult, are reduced carrier generation near the rear contact (when the real beam profile is used; see fig. 4) and the injection of carriers into this region from the rear contact or from the bulk of the dielectric. The fact that the observed collected currents are higher when a negative voltage is applied to the front contact than when a positive voltage is applied suggests the possibility that injection from an irradiated region of the dielectric is greater than that from a metallic contact.

V. CARRIER-ENHANCED CONDUCTIVITY STUDIES - PARTIAL PENETRATIONS

Carrier-enhanced conductivity (CEC) is almost a tautological phrase, since all conductivity requires carriers and any increase in carrier concentration will enhance conductivity. Radiation-induced conductivity, field-enhanced conductivity, and thermally-stimulated conductivity are all forms of increased conductivity resulting from increased carrier concentrations. However, we reserve the phrase "carrier-enhanced conductivity" for specific cases in which extra carriers are introduced from a contact or from an adjacent irradiated (RIC) region. Because of space charge limitations, we assume that the number of extra carriers injected from a metal contact or from a RIC region is not large enough to alter the carrier mobility or to deviate from a shallow-trap controlled dependence (that is, recombination with positive trapped charge can be neglected). The main reason that this small number of carriers may be important is that in high field regions, conductivities may be very low after enough time has elapsed to drain free or easily excited carriers from the dielectric. Unless external charge or ionizing radiation are introduced to provide more carriers, the conductivity of a dielectric in a field can decrease by orders of magnitude in a few hours. In the previous section, we discussed dielectrics with carriers introduced nonuniformly by ionizing radiation. The effects of charge injection from contacts or migration of charge from adjacent, heavily ionized regions

were observed in the less heavily ionized regions. Such effects are probably even more important in regions of low free-carrier concentrations (for example, nonirradiated or high field regions).

Two approaches were used to study the CEC problem affecting conduction in the unirradiated region. In one approach, the LWPCHARGE computer program, capable of treating fixed front-surface biases and carrier kinetics, was applied to partial penetrations of thin-Kapton samples and compared with experimental results (ref. 7). In the other approach, an analytical model with field injection from the RIC region was used to determine mobility in the unirradiated region (ref. 14). Additional results from both approaches are discussed below.

A. LWPCHARGE Code Results for Partial Penetrations

Carrier kinetics were included in the code by assuming the conductivity to be $-\mu'\rho$, where μ' is the mobility and ρ is the excess-charge density deposited by the primary beam. Therefore, the drift contribution to the current is determined by multiplying this conductivity by the electric field intensity. Diffusion was neglected (as in ref. 3). The dose and excess charge deposition rates were computed by using the Monte Carlo transport code (ref. 1) as in figure 4.

The following partial penetration results were obtained for the 6.4-μm thin Kapton, using 1 nA/cm^2 beams of energies 5, 10, 15, 20, and 28 keV, with zero bias on the sample. The mobility was assumed to be $\mu' = 10^{-15}$ m^2/V-s.

For each beam energy, table 1 shows the range, substrate current J_2, potential minimum V_m, position X_m of the minimum, and the approximate time scale for the transient. We see that the substrate current becomes significant when the range is greater than about half the sample thickness. (This "threshold effect" is in accord with the literature.) The potential minimum becomes deeper as deeper penetration occurs but starts to weaken after the sample has been penetrated. Its position progresses from zero to the midpoint of the sample with increasing beam energy. The time scale for establishing equilibrium is longest for the low-energy beam (about 20,000 s); the time diminishes as the beam energy (and depth of penetration) increases.

Experimental results of electron beams on 6.4-μm Kapton (normalized to 1 nA/cm^2 incident beam currents, assuming proportional scaling for small differences in beam current) are shown in table 2. (Comparing these results with those of table 1 indicates close agreement of J_2 in the case of penetrating beam (28 keV) and poor agreement in cases of the lower energy beams. However, the choice of $\mu' = 10^{-15}$ m^2/V-s in the computer model is probably low by a factor of three (as seen in the next section) to seven (as seen in Subsection IV B). If mobility is increased by a factor of three, the current J_2 collected at the back contact in the 15-keV case should also increase in magnitude, thereby coming into closer agreement with the experimental value (-0.12 nA/cm^2). The time scales should be reduced by nearly a factor of three (ref. 6), and the resulting ~900- and 300-s theoretical values are in much closer agreement with the 400- and 175-s experimental values for 15- and 28-keV beams, respectively. If the higher value of mobility ($\mu' = 7 \times 10^{-15}$ m^2/V-s) is used, the calculated results are even closer to the experimental results.

The fact that the model (if $\mu' = 3-7 \times 10^{-15}$ m^2/V-s) is in such close agreement with experimental results, even without a diffusion contribution of carriers to the

unirradiated region, indicates that (at least for low beam current densities) diffusion may be unimportant compared to the field-assisted drift of charge from the irradiated region. Before this statement can be confirmed, more comparison with experimental data, a better modeling of the mobile carrier concentration in the RIC region (to include ionization from the beam), and a successful incorporation of a diffusion term into the model must be carried out. However, in contrast to semiconductors (for which diffusion is significant), the diffusion of carriers in dielectrics should be small compared to the drift field injection, since free carrier concentrations and mobility are extremely low in dielectrics. Since field injection dominates diffusion and since diffusion could only have an effect in a charge-depleted region (that is, in a strong field region where field injection is more important), charge diffusion in dielectrics might reasonably be neglected.

B. Analysis of Thick Kapton Samples

In the thin Kapton samples analyzed above, the conduction processes are dominated by radiation-induced conductivity, with space-charge effects playing a lesser role. However, in beam irradiation experiments performed on 127-μm Kapton samples (ref. 2) (which are thick compared to the range of 2 to 18 keV electrons—a few microns), the RIC region is thin compared to the nonirradiated region. In these samples, the properties of the nonirradiated region are expected to control the current-voltage characteristics of these materials.

Yadlowsky and Hazelton (ref. 14) have recently analyzed the experimental results of Hazelton et al. (ref. 2) and Adamo et al. (ref. 15) in light of space-charge-limited-flow models, a field-enhanced conductivity model (Poole-Frenkel effect), Schottky barrier models, and a combination of Poole-Frenkel conduction and space-charge-limited currents. The classical expression

$$J_S = - \epsilon\mu \frac{9}{8} \frac{V^2}{L^3} \tag{7}$$

for the space-charge-limited current through a dielectric sample appears to properly represent the functional dependence observed by Adamo et al. (ref. 15) for current flow between biased electrodes in an unirradiated sample. For an irradiated sample, equation (7) can be made to fit the experimental current-voltage results only if an order of magnitude variation in the value of the mobility is made (ref. 14). Yadlowsky and Hazelton (ref. 14) also found that the current voltage dependence can be represented by the other models mentioned above, but not satisfactorily. For example, in each case, a nonphysical beam energy dependence for the dielectric permittivity, ϵ, had to be assumed to obtain a functional fit. In addition, the value of the permittivity required to fit the data was five to six times the accepted value in some cases. These results led to the conclusion that these models are unsatisfactory in their usual forms. However, satisfactory results were obtained using a modified version of the space-charge-limited current model (ref. 14).

In the usual form of this model, the field is assumed to be zero at the injection plane. The new model allows the field to have a finite value, E_0, at the virtual injection electrode, which is taken to be the point at which the primary beam current vanishes. Relatively good fits were obtained with a simplified version of this model, emphasizing the importance of including injection electrode effects in the analysis. This model accounts for beam energy dependence effects in a natural way and explains the difference between the Adamo et al. (ref. 15) biased electrode

measurements, for which injection occurs at the metal contact, and the irradiated dielectric studies, for which injection occurs from an ionized region of the dielectric. Measurements and analysis are required to determine whether space-charge effects in the injection region or field-enhanced conductivity in the unirradiated region dominate the charge transport process in the bulk of the dielectric.

Experimental results were used to determine values of the injection fields E_0 (ref. 14). These values, in turn, were used here to calculate values for the trap-modulated mobility μ'. Table 3 displays both sets of values for beam energies of 8, 12, 16, and 18 keV. The values of μ' in table 3 suggest computer input values of μ' in Subsection V B. For consistency, the computer model (with the new value of μ') should also predict the values of E_0 deduced from the experiment results.

C. Discussion of CEC Results

To understand the experimental results of a nonpenetrating electron beam incident on Kapton samples, it is necessary to invoke field-assisted injection of carriers from the irradiated region into the nonirradiated region. An analytical space-charge limited model, with a nonvanishing field at the injection plane (the edge of the irradiated region) has provided results consistent with both experimental data and a preliminary computer carrier model. The conditions under which space-charge limited flow occurs (for example, free carrier density inadequate to neutralize injected carriers) must be investigated. A comparison of other experimental results with the present computer model will provide better material parameters and will indicate where modifications to the model and to the space-charge limited current theory are required. At early times in a charging experiment, free carriers in the dielectric bulk may be too numerous for space-charge limitations to occur. On the other hand, if field injection from an irradiated region (greater than from a metal contact if our RIC results are valid) is high enough, the injected carriers may dominate all other carrier sources.

Comparison of Kapton with different materials such as Teflon (in which field-injected electrons would compete with the more mobile holes) or with ceria-doped-microsheet (in which the high concentration of free carriers resulting from the cerium ions could prevent space-charge limiting) would be very useful in testing the present theory and model.

VI. IMPLICATIONS OF THIS WORK

The use of penetrating beams on a thin, metallized dielectric establishes conditions that are closely analogous to those in the RIC region of a nonpenetrated dielectric. For instance: a 1 nA/cm^2 beam of 28 keV electrons penetrating a 6.4-μm dielectric film deposits nearly 45 mW/cm^3 throughout the sample. On the other hand, a nonpenetrating 1-nA/cm^2 beam incident on a free surface dielectric will charge that surface to within approximately 2 keV of the beam energy (at which point secondary emission balances the incident beam). If most of the 2 keV per electron is deposited in the first 0.2 μm, the deposited power density is 100 mW/cm^3. The dose rate in, and therefore the conductivity of the two regions will be very similar. The deposited excess charge density will be greater in the 0.2-μm layer, but because the distance the excess charge must travel before removal from the layer is less in the thin layer than in the thin film (<0.2 μm vs <3.2 μm), the current densities (and perhaps the potential profiles) should also be similar.

The electric field at the back contact of a thin dielectric with its front contact biased to +45 V and $J_B \approx 0.65$ nA/cm² in figure 2 is zero. This back contact corresponds to the zero field region in the RIC volume near the nonirradiated portion of a thick dielectric. This area of the RIC region, then, is equivalent to an electrode in the RIC region. The positively biased front contact of a thin metallized film corresponds to the carrier sink of an irradiated Kapton sample free surface, for which secondary emission removes surface electrons. Changing the bias on this front contact (for a fixed beam current) varies the position of the zero field region. This change permits the RIC region to be probed, allowing a more accurate determination of its material parameters. Other conditions may need to be established for Teflon, in which holes are the majority carrier and for which the irradiated surface (when positive) is therefore an injecting electrode. Materials in which both holes and electrons have comparable mobility or in which conditions are other than those assumed here for Kapton, must be examined in a similar manner to determine the appropriate experiments for establishing material parameters.

Because of nonuniformities in fields and potentials in the RIC region, and because of their strong dependence on changes in beam current density and external applied bias (corresponding to changes in the experimental conditions of a non-penetrating beam experiment), incorrect values for material parameters and even for functional dependence (in both irradiated and nonirradiated regions) are likely to be inferred unless a computer model is used to unravel the problem. Many conclusions from past work are suspect for this reason, or, if correct, they may not pertain to conditions that are applicable to dielectric discharges. Although the data may be good, it must be reevaluated in many cases. Such problems account for many of the deviations observed in experimentally determined parameters (such as dose dependence of conductivity, and so on). Future work must be carried out only after careful study of the conditions to be simulated and after testing of a model to correctly interpret the results.

Once appropriate models are tested and true irradiated material parameters are evaluated, a more valid assessment of breakdown conditions and probability can be made. Variation of material and beam parameters in the computer model can then be used to determine the best means of preventing discharge conditions.

VII. SUMMARY

Although experimental measurements of RIC are available, it is still necessary to use a theoretical model to correctly interpret them. A model for RIC is described here, based on steady-state solutions of general kinetic equations for electrons and holes. An assumption is made that the holes are instantaneously trapped into deep traps, while the electrons hop from shallow trap to shallow trap and are described as quasi-free with a lowered "trap-modulated" effective mobility. This simplifies the description of the system to the Poisson equation plus a single transport equation for the electrons. Parameters required by the model include mobility, pair generation rate, and excess-charge deposition rate.

Raw data on a 6.4-µm sample of Kapton, taken at ±196-V and ±45-V bias penetrated by a 28-keV incident electron beam energy, are considered for interpretation. Of prior concern was the approximately 60-40 split of the rear and front currents observed at zero bias. Moreover, the experimental values inferred for the RIC are polarity dependent. However, the present model can explain the 60-40 split at zero bias, by appropriate choices of dose and excess charge deposition profiles, and by a particular choice of mobility, can match the experimental currents under bias.

Injection at the cathode contact is required to allow matching of the experimental currents. Under conditions of high injection, the shapes of the electron concentration and potential are monotonic and no strong fields are present (fig. 6). The mean value of the RIC turns out to be consistent with values in the literature. The polarity dependence of the experimentally observed currents is explained in terms of spatial variations in charge deposition, internal conductivities, and fields.

The problem of partial penetrations is also considered. The LWPCHARGE code, including carrier kinetics, was used to describe CEC effects. Transient solutions were obtained for partial penetrations of the thin-Kapton sample with beam voltages less than 28 kV. Significant rear currents were predicted when the penetration depth was half the thickness (threshold effects). For low beam voltage, the transient time is very long. As the beam voltage increases, the transient time decreases and the (negative) potential minimum deepens, until full penetration is achieved. The zero-bias, rear-front current split is calculated to be 63-37.

Field extraction of charge from the RIC region is assumed in a space-charge limited current model to interpret experimental results obtained on thick (5-mil) Kapton samples with a free front surface. From our various models, an inferred value of effective mobility ($\mu' \approx 3\text{-}7 \times 10^{-15}$ m^2/V-s), which is consistent with the literature, has been obtained for both RIC and CEC regions.

REFERENCES

1. L. W. Parker et al., "Charging Characteristics and Electrical Parameters of Spacecraft Dielectrics Under Electron Irradiation," Lee W. Parker, Inc., Final Report, INTELSAT Contract INTEL-046, June 1982.

2. R. C. Hazelton et al., "Effect of Material Parameters on the Charging Characteristics of Irradiated Dielectrics," IEEE Transactions on Nuclear Science, NS-28, 1981, pp. 4541-4546.

3. K. Labonte, "Radiation-Induced Charge Dynamics in Dielectrics," IEEE Transactions on Nuclear Science, NS-29, 1982, pp. 1650-1653.

4. R. C. Hughes and R. J. Sokel, "Computation of Photoconductivity in Insulators in the Space Charge and Recombination Regime: Application to PbO Films," Journal of Applied Physics, Vol. 52, 1981, pp. 6743-6746.

5. R. Sokel and R. C. Hughes, "Numerical Analysis of Transient Photoconductivity in Insulators," Journal of Applied Physics, Vol. 53, 1982, pp. 7414-7424.

6. J. N. Churchill, F. E. Holmstrom, and T. W. Collins, "Dynamic Model for e-Beam Irradiation of MOS Capacitors," Journal of Applied Physics, Vol. 50, 1979, pp. 3994-3999.

7. L. W. Parker, "Theoretical Investigations of Radiation-Induced and Carrier-Enhanced Conductivity," Lee W. Parker, Inc., Final Report, INTELSAT Contract INTEL-277, 1983.

8. L. N. Oliveira and B. Gross, "Space Charge Limited Currents in Electron-Irradiated Dielectrics," Journal of Applied Physics, Vol. 46, 1975, pp. 3132-3138.

9. W. E. Spear, "Electron Bombardment Effects in Thin Dielectric Layers," _Proc._, _Physical Society, London_ B68, 1955, pp. 991-1000,____

10. F. C. Aris, P. M. Davies, and T. J. Lewis, "Electron-Beam-Induced Conduction in Dielectrics," _Journal Phys. C: Solid State Phys._, Vol. 9, 1976, pp. 797-808.

11. S. Matsuoka et al., "Accumulated Charge Profile in Polyethylene During Fast Electron Irradiations," _IEEE Transactions on Nuclear Science_, NS-23, 1976, pp. 1447-1452.

12. B. Gross, R. M. Faria, and G. F. L. Ferreira, "Radiation-Induced Conductivity in Teflon Irradiated by X-Rays," _Journal of Applied Physics_, Vol. 52, 1981, pp. 571-577.

13. A. R. Frederickson, "Charge Deposition, Photoconduction, and Replacement Currents in Irradiated Multilayer Structures," _IEEE Transactions on Nuclear Science_, NS-22, 1975, pp. 2556-2561.

14. E. J. Yadlowsky and R. C. Hazelton, "Conduction Processes in Kapton H Irradiated by an Electron Beam," _IEEE Transactions on Nuclear Science_, NS-31, December 1983.

15. R. C. Adamo, J. E. Nanevicz, and N. Grier, "Conductivity Effects in High-Voltage Spacecraft Insulating Materials," _Proceedings of the Spacecraft Charging Conference_, AFGL-TR-77-0051/NASA TMX-73537,669, 1977.

Table 1. Partial Penetrations at Zero Bias

Energy (keV)	Range (μm)	J_2 (nA/cm^2)	V_m (V)	X_m (μm)	Time Scale (s)
5	0.4	-6×10^{-5}	-2	0.4	2×10^4
10	1.4	-3×10^{-3}	-11	1.2	3,400
15	2.8	-0.042	-30	2.2	2,500
20	4.4	-0.21	-45	2.8	700
28	>6.4	-0.63	-31	3.0	700

Table 2. Experimental Results for
1 nA/cm^2 Electron Beams on
6.4 μm Kapton

Beam Energy (keV)	J_2 (nA/cm^2)	Time Scale
15	-0.12	400
25	-0.48	
28	-0.61	175

Table 3. Electrical Parameters for
Thick Irradiated Kapton

V_B (keV)	E_0 (V/cm)	μ, (m^2/V-s)
8	4.7×10^5	3.1×10^{-15}
12	5.2×10^5	2.8×10^{-15}
16	3.7×10^5	4.3×10^{-15}
18	2.8×10^5	1.9×10^{-15}
Average	$4.0 \pm 1.2 \times 10^5$	$3.1 \pm 1.2 \times 10^{-15}$

Figure 2. Collected Currents vs Electron Beam Current With +45 V Applied Bias

Figure 1. Collected Currents vs Electron Beam Current Entering a Dielectric (A +196 V bias applied to front surface; positive currents are defined as electrons moving toward the right; superscripts indicate polarity of the bias)
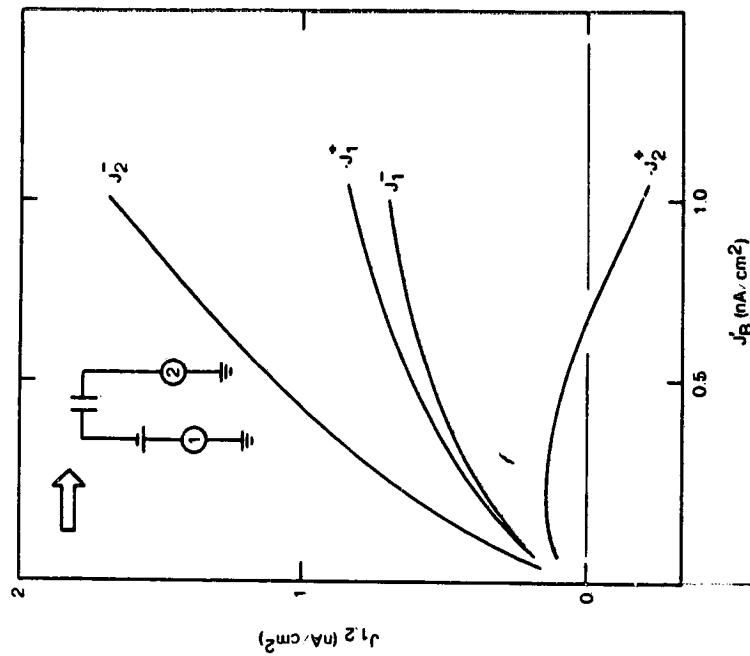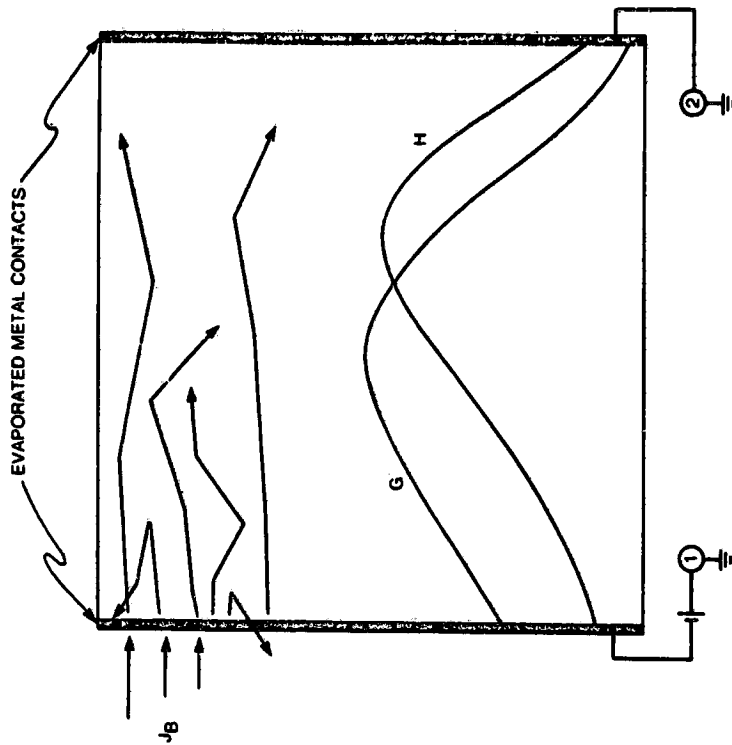
587

Figure 4. Schematic of Experiment: Electron Beam Incident on Biased Front Contact (Number 1), Electrons Scattered and Deposited Within Dielectric (energy and charge deposition rate profiles represented by G and H)

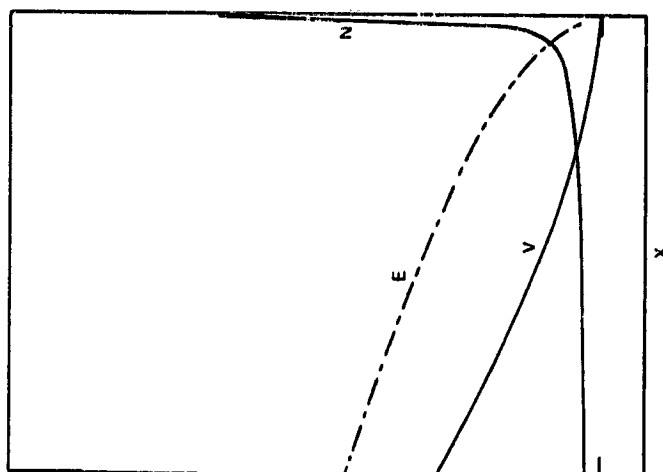

Figure 3. Primary Flux From Monte Carlo Transport Code

Figure 6. Electrical Parameters Determined by Computer Fit to Experimental Data, Assuming Constant G and H (+200 v applied to front contact and high electron injection at back contact)
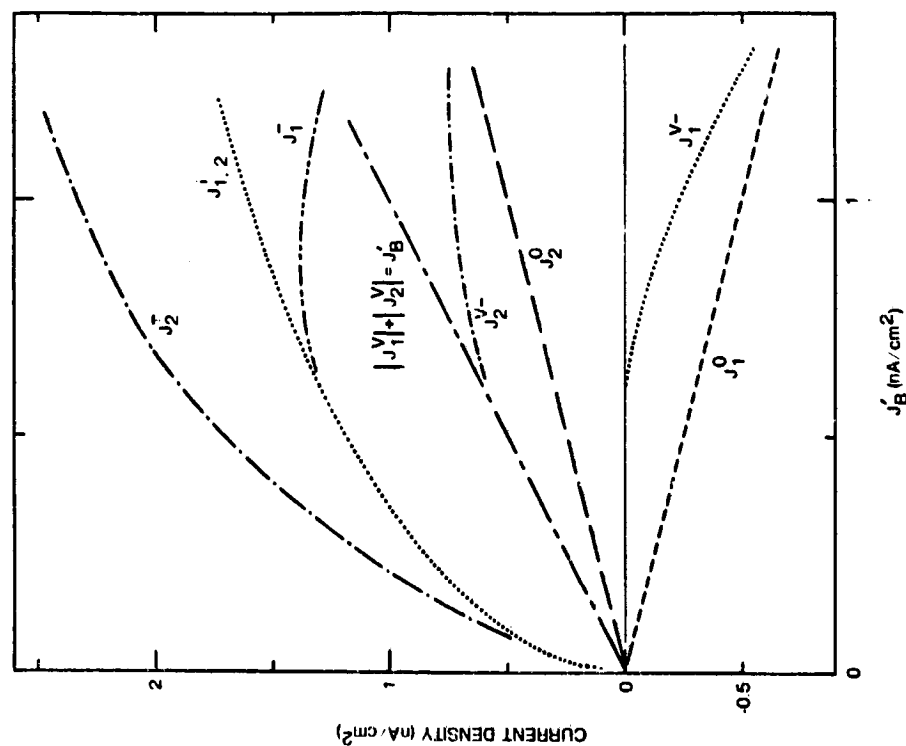

Figure 5. Electrical Parameters for Dielectric Exposed to an Electron Beam (G and H Constant) With Electric Field E, Potential V, and Drift-Diffusion Flux F_{DD} Resulting From Incident Flux F

Figure 8. Collected Currents $J_{1,2}^+$ vs Electron
Beam Current J_B' Modelled With a Positive
Applied Bias, Assuming Constant G and H

Figure 7. Collected Currents $J_{1,2}^-$ vs Electron
Beam Current J_B' Modelled With a Negative
Applied Bias, Assuming Constant G and H
(constituent parts result from injection
at contacts $J_{1,2}^i$ and from motion
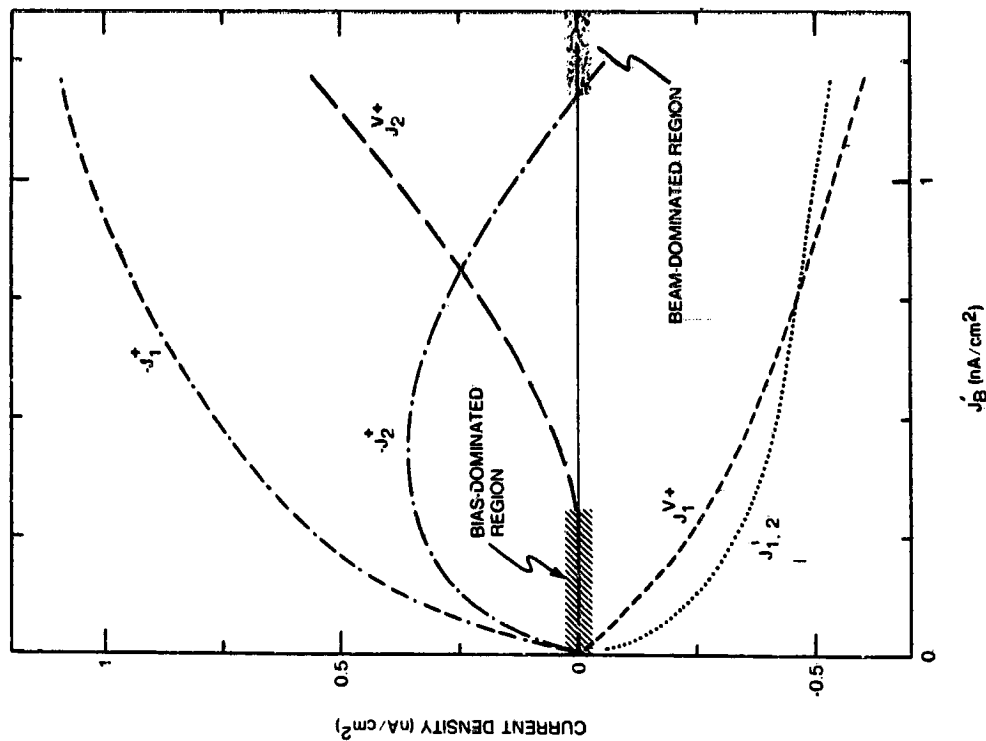of beam-deposited charge $J_{1,2}^V$)